Study on the weakening of stator cogging torque of modular motors by gap offsets

CAIXIA TAO [1], YAOGENG ZHANG [1✉], FENGYANG GAO [1], JIANGANG ZHANG [2]

[1]*School of Automation and Electrical Engineering, Lanzhou Jiaotong University*
Gansu Province, China

[2]*School of Mathematics and Science, Lanzhou Jiaotong University*
Gansu Province, China
e-mail: {1733425004/✉ 1973842201/2633252283/3551037}@qq.com

Abstract: Two schemes have been developed to reduce the cogging torque generated by the gap between the stator modules of the modular permanent magnet synchronous motor. These schemes involve shifting the gap position to change the phase of the cogging torque, thereby eliminating some of its components and reducing its magnitude. Finite element simulation was used to verify the cogging torque of E and C type modular motors using two different schemes. The effect of the offset gap on electromagnetic performance and motor vibration noise was also analysed. The results indicate that both schemes weaken the cogging torque without significantly affecting the electromagnetic performance of the motor or increasing vibration noise.

Key words: cogging torque, modular motor, permanent magnet synchronous motor, vibration and noise

1. Introduction

The modular stator structure has been adopted for permanent magnet synchronous motors (PMSMs) in wind power, electric vehicles, and aerospace due to the increasing demand for reliability and safety [1–4]. Additionally, the difficulty in manufacturing large one-piece motors has led to the increased use of modular stators. The stator of the motor can be designed in various structures. Some common designs include the T-module [5], which improves slot fullness, and the E and C-modules [6], which reduce weight. Additionally, the stator can be designed with a segmented structure for the stator yoke and teeth [7], which simplifies the assembly process. Literature [8, 9] has analysed the influence of various parameters on the performance of motors, including stator module splice shape, number of modules, stator or rotor eccentricity, permanent magnet machining error, material property error, and unequal spacer spacing.

However, the modular stator will inevitably have gaps between modules during assembly due to its structural limitations. In literature [10], the effect of adding an isolation gap between the modules is analysed. It is found that this can attenuate the low harmonics of the motor's magneto-dynamic potential and significantly reduce the eddy-current losses of the permanent magnets. Literature [11–13] suggests that increasing the gap between modules can improve the average torque of the motor. However, this also results in increased extra cogging torque and torque pulsation. The conditions for increasing the average torque of the motor have not been explored. In literature [14], it is stated that the pole-slot fit affects the average torque increased by the inter-module gap, but the mechanism of change is not analysed. Literature [15] analyses the mechanism of the effect of pole slot fit on the gap and explains the relationship between pole slot fit and gap.

Literature [16] investigated the optimal width of various stator module structures with different pole-slot fits. However, it did not include an analysis of the electromagnetic vibration of the motor. Literature [17] analysed the clearance of the block structure of stator yoke and tooth segments and concluded that a smaller assembly clearance is better. However, this may increase the difficulty of the machining process and assembly. According to Literature [18], the cogging torque of T-type modular motors can be reduced by using a closed slot, although this may result in a more complex assembly. Literature [19] proposed an additional stator yoke component structure with six non-magnetic materials embedded in the stator yoke section. This structure reduces the high harmonics of the air-gap flux density of the fractional-slot toothed-centre windings by means of a flux barrier. However, the assembly is more complicated, and the strength of the mechanical structure has not been analysed. Current research on modular motors primarily focuses on improving motor efficiency, optimizing structure and reliability, and studying electromagnetic characteristics. There is less emphasis on reducing cogging torque.

Cogging torque is the torque generated by the interaction between the permanent magnet and the iron core when the permanent magnet motor rotates in the power-off state. It can have a serious impact on the stability of the PM motor and is also a partial source of noise. Two model schemes are proposed to reduce the cogging torque of a modular motor by utilizing its own structure. Firstly, the theoretical analysis of the schemes is carried out, and then the finite element method is used to simulate and verify the 10-pole, 12-slot C-type and E-type modular PM synchronous motors, and other important parameters of the motors are analysed, and finally, the electromagnetic vibration of the motors is simulated and analysed to verify the feasibility and superiority of the schemes. The motor model can be used for large motor builds and where reliability is critical.

2. Modular motor cogging torque optimisation scheme

2.1. Introduction of modular motor stator models

The modular motor stator structure typically utilises T-type, U-type, E-type, and C-type designs. T-type and U-type designs aim to minimise the gap between modules by incorporating dovetails between them. U-type stator modules use magnetic material in the connecting block, while E-type and C-type modules have a magnetic gap that is usually maintained at a specified distance, as illustrated in Fig. 1.
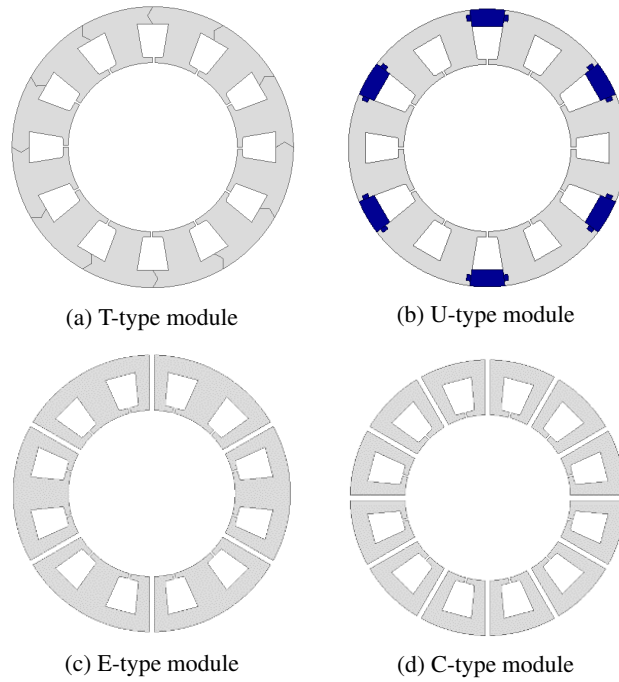
(a) T-type module   (b) U-type module

(c) E-type module   (d) C-type module

Fig. 1. Common modular motor stator structure diagram

2.2. Analysis of cogging torque

Cogging torque is the torque generated by the magnetic field of the permanent magnets interacting with the armature when the motor is in an open circuit state. The general expression for cogging torque T_{cog}, without the use of slanted slots and inclined poles, can be obtained as stated in the Literature [20].

$$T_{cog} = T_{N_S n} \sin(N_s n \alpha), \tag{1}$$

where: n is the number of harmonics, $T_{N_S n}$ is the amplitude of the cogging torque for the n-th harmonic, N_s is the number of cycles of the cogging torque when the motor is rotated through $360°$, and α is the angle of the relative position of the stator and rotor.

For one-piece motors, the frequency of the cogging torque is the least common multiple of the number of stator slots and the number of pole pairs. For modular motors, the gap between the modules causes a change in the symmetrical structure, which further alters the symmetry of the stator magnetic circuit, and therefore the frequency of the cogging torque is also altered and changes to the least common multiple of the number of symmetrical structures and the number of pole pairs in the stator [21].

Since the cogging torque of a motor can be viewed as a superposition of the cogging torque caused by each stator cogging slot, for modular motors, the total cogging torque can be viewed as a superposition of the two parts of the cogging torque, the stator cogging slots and the gap between the modules [22].

Therefore, the reduction of the cogging torque for modular motors can be broadly classified into three methods, which are:

1. Weaken the cogging torque caused by the stator tooth groove;
2. Weakening of the cogging torque caused by the gap between modules;
3. Offsetting the cogging torque caused by both the stator cogging and the module gap weakens the cogging torque.

For method 1, due to the use of modular stator, the cogging torque can be weakened in the form of closed slots for motors similar to T-block, but it will weaken the motor output efficiency [23]. Otherwise, the method of optimising the cogging torque is no different from that of a normal motor. Therefore, for the weakening of cogging torque, the schemes adopted in this paper are mainly method 2 and method 3.

2.3. Optimisation of programme design

Due to the similar structure of E-type and C-type modules, the following analysis is carried out using E-type modules as the optimisation object.

2.3.1. Changing phases to weaken the gap-gear torque

For the cogging torque that weakens the inter-module gap, from Eq. (1), the n-th harmonic of the cogging torque of a permanent magnet motor can be regarded as a sinusoidal function, and all the gaps can be classified into two groups, as shown in Fig. 2.
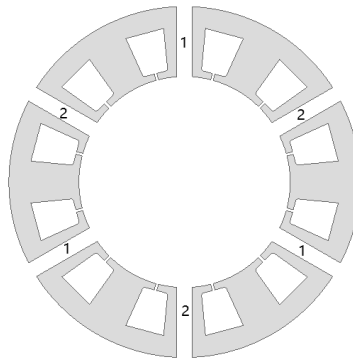

Fig. 2. Gap cogging torque grouping

The cogging torque due to each set of clearances can be expressed as T_{cog1} and T_{cog2}, i.e., the cogging torque is

$$T_{\text{cog}} = T_{\text{cog1}} + T_{\text{cog2}}, \tag{2}$$

$$T_{\text{cog1}} = T_{N_s n1} \sin(N_s n\alpha), \tag{3}$$

$$T_{\text{cog2}} = T_{N_s n2} \sin(N_s n\alpha), \tag{4}$$

where $T_{N_S n1}$ and $T_{N_S n2}$ are the respective amplitudes of the two groups.

From Eqs. (2), (3) and (4), the total cogging torque can be reduced if the sinusoidal type functions T_{cog1} and T_{cog2} cause the cogging torque generated by the two sets of gaps to partially offset each other by changing their phases.

For changing the phase of T_{cog1} and T_{cog2}, the two sides of the reverse offset gap can be used to make two kinds of modules respectively, and finally spliced together, as shown in Fig. 3 from Formulas (2), (3) and (4) can be seen, when sinusoidal functions T_{cog1} and T_{cog2} by changing their phase, so that the two sets of gaps produced by the cogging t torque partially offset each other, can reduce the total cogging torque.

To change the phases of T_{cog1} and T_{cog2}, the two modules can be fabricated separately by using bilaterally reverse offset of gaps and finally spliced together as shown in Fig. 3.
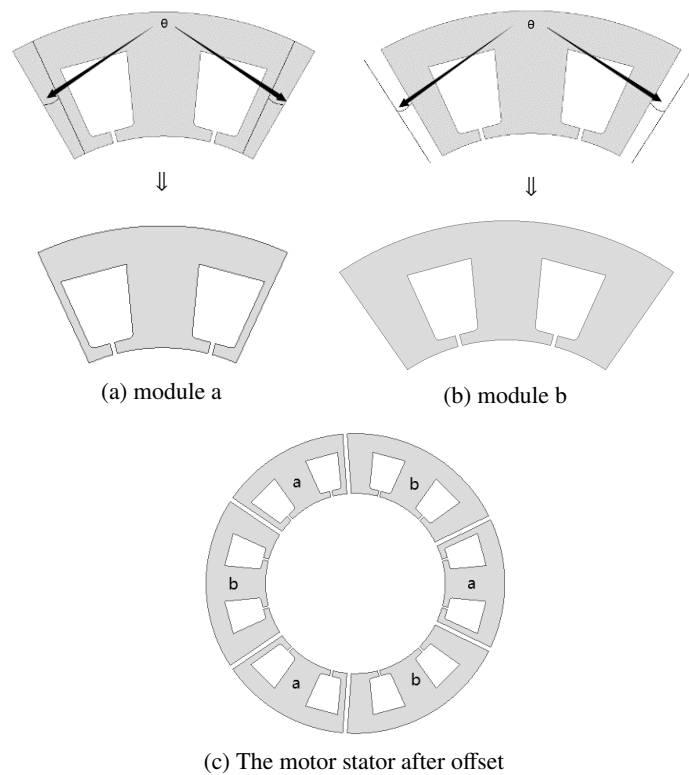

(a) module a   (b) module b

(c) The motor stator after offset

Fig. 3. Bilaterally reverse offset of gap

T_{cog1}, T_{cog2} can be expressed as

$$T_{\text{cog1}} = T_{N_S n1} \sin\left[N_s n(\alpha + \theta)\right],\tag{5}$$

$$T_{\text{cog2}} = T_{N_S n2} \sin\left[N_s n(\alpha - \theta)\right],\tag{6}$$

where θ represented in Fig. 3.

Since the two parts are essentially the same, an approximation can be made.

$$T_{N_S n 1} = T_{N_S n 2}.$$

That is, the total cogging torque is

$$T_{\text{cog}} = \sum_{n=1}^{\infty} T_{N_S n 1} \sin\left[N_s n(\alpha + \theta)\right] + \sum_{n=1}^{\infty} T_{N_S n 2} \sin\left[N_s n(\alpha - \theta)\right]$$

$$= \sum_{n=1}^{\infty} T_{N_S n 1} \sin\left(N_s n \alpha\right) \cos(N_s n \theta). \tag{7}$$

From Eq. (7), if the two parts cancel out completely, there are

$$\cos\left(N_s n \theta\right) = 0 \Rightarrow \theta = \frac{\pi}{N_S n}. \tag{8}$$

Finite element simulations were later used to further determine the exact range of θ.

2.3.2. Backlash and cogging counteract each other to reduce cogging torque

Since the gap between the modular motor modules is unavoidable, the gap can be used to weaken the original cogging torque. The cogging torque T_{I} generated by the gap and the cogging torque T_{II} generated by the stator cogging are divided into two parts as shown in Fig. 4.
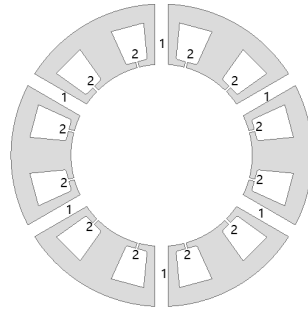

Fig. 4. Cogging torque grouping

The total cogging torque T_{cog} consists of two superimposed parts and is expressed as

$$T_{\text{cog}} = T_{\text{I}} + T_{\text{II}}, \tag{9}$$

$$T_{\text{I}} = T_{N_S n \text{I}} \sin(N_{s\text{I}} n \alpha), \tag{10}$$

$$T_{\text{II}} = T_{N_S n \text{II}} \sin(N_{s\text{II}} n \alpha), \tag{11}$$

where $T_{N_S n \text{I}}$ and $T_{N_S n \text{II}}$ are the respective amplitudes of the gap and stator cogging torques, and $N_{s\text{I}}$ and $N_{s\text{II}}$ are the number of cycles of the gap and stator cogging torques.

From Eq. (10), the gap causing cogging torque T_{I} can be expressed as:

$$T_{\text{I}} = \sum_{n=1}^{\infty} T_{N_S n \text{I}} \sin\left[N_{s\text{I}} n(\alpha + \theta)\right]. \tag{12}$$

Changing the phase of the gap-slot torque, i.e., bilaterally forward offset of gaps, can make the processing of the block easier, and only one kind of module needs to be made, as shown in Fig. 5.

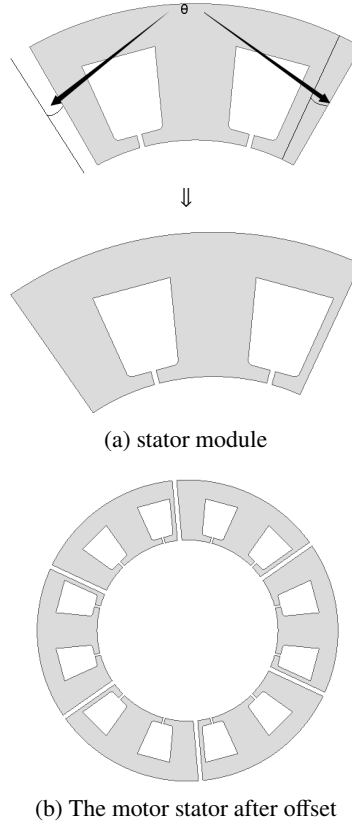(a) stator module

(b) The motor stator after offset

Fig. 5. Bilaterally forward offset of gap

Here, since neither the amplitude nor the period are necessarily equal, no approximation is made and the total cogging torque is

$$T_{\text{cog}} = \sum_{n=1}^{\infty} T_{N_S n\text{I}} \sin\left[N_{s\text{II}} n(\alpha + \theta)\right] + \sum_{n=1}^{\infty} T_{N_S n\text{II}} \sin(N_{s\text{II}} n\alpha). \tag{13}$$

Finding the magnitude of θ can be done by finding the extremes of Eq. (13) that take the mean value over a period, i.e., finding the extremes of Eq. (14).

$$\int_{0}^{t} \left| \sum_{n=1}^{\infty} \left\{ T_{N_S n\text{I}} \, \sin\left[N_{s\text{I}} n(\alpha + \theta\right] + T_{N_S n\text{II}} \sin(N_{s\text{II}} n\alpha) \right\} \right| \mathrm{d}x, \tag{14}$$

where t is the period of the total cogging torque, i.e., the least common multiple of the period of the gap cogging torque and the period of the cogging torque produced by the stator cogging.

For ease of solution take

$$\theta \approx -\frac{3\pi}{4N_{sI}n} - \frac{\pi}{2N_{sII}n}. \tag{15}$$

The finite element method was later used to further determine the exact range of θ.

3. Verification of cogging torque simulation

3.1. Simulation model construction and θ angle determination

In this paper, a modular permanent magnet synchronous motor with 10 poles and 12 slots is used as the simulation object, the rotor is of V type interior permanent magnet rotor and NdFe35 is used as the permanent magnet. Table 1 displays the other design parameters of the motor.

Table 1. Motor design parameters

Motor parameter	Data value
Number of pole-pairs	5
Number of slots	12
Stator outer radius	135 mm
Inner radius of stator	81 mm
Rotor outer radius	80 mm
Inner radius of rotor	45 mm
Stator slot top radius	86 mm
Radius of stator slot bottom	118 mm
Stator slot top width	20 mm
Stator slot bottom width	30 mm
Stator slot opening	2 mm
Permanent magnet thickness	6.8 mm
Rated speed	600 RPM
Motor parameter	data value
Axial length	100 mm
Gap width of E-type module	5 mm
Gap width of C-type module	3.3 mm
Rated power	5.5 KW
Rated current	11.5 A

Finite element simulations of motors are usually performed using Maxwell [24]. The simulation involves changing the phase to weaken the gap-slot torque and the gap-slot offset to weaken the cogging torque for the E and C modules, respectively. The model is constructed using finite

element software Maxwell, as shown in Fig. 6. In the mesh discretisation of the model, the air gap was divided into four layers of 0.25 mm each, and the rest of the motor part was 10 mm. Since the mesh discretisation is similar for each model, in this paper we take the unoffset C-type as an example and the generated mesh is shown in Fig. 7, with a total of 39 710 meshes, of which 20 228 meshes are divided at the air gap.
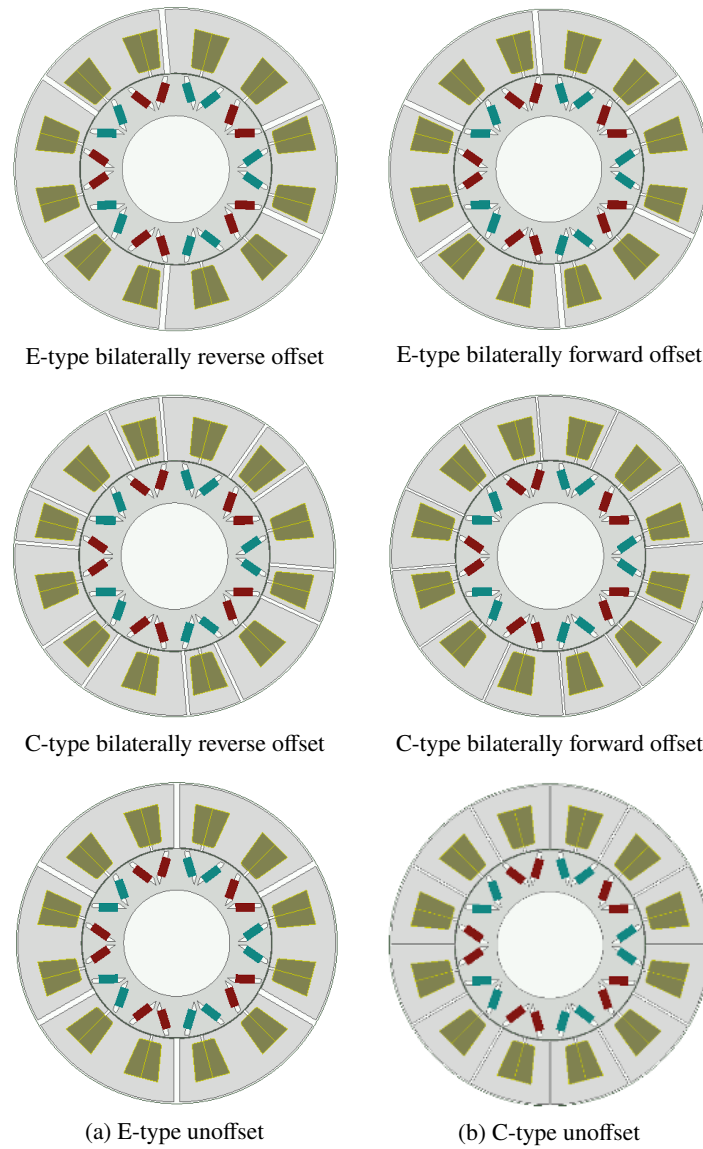

E-type bilaterally reverse offset   E-type bilaterally forward offset

C-type bilaterally reverse offset   C-type bilaterally forward offset

(a) E-type unoffset   (b) C-type unoffset

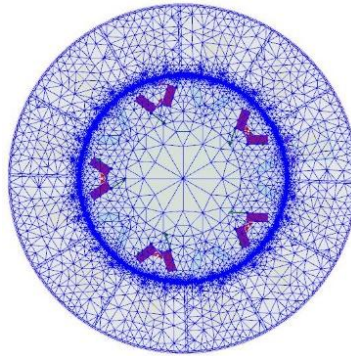Fig. 6. Modular motor simulation model diagram

Fig. 7. C-type unoffset mesh discretisation

The value of θ is determined using Eqs. (8) and (14). Subsequently, the finite element method is employed to generate a series of isotropic θ values for simulation. The obtained θ value is used as the centre with a tolerance of $0.1°$, as illustrated in Fig. 8.
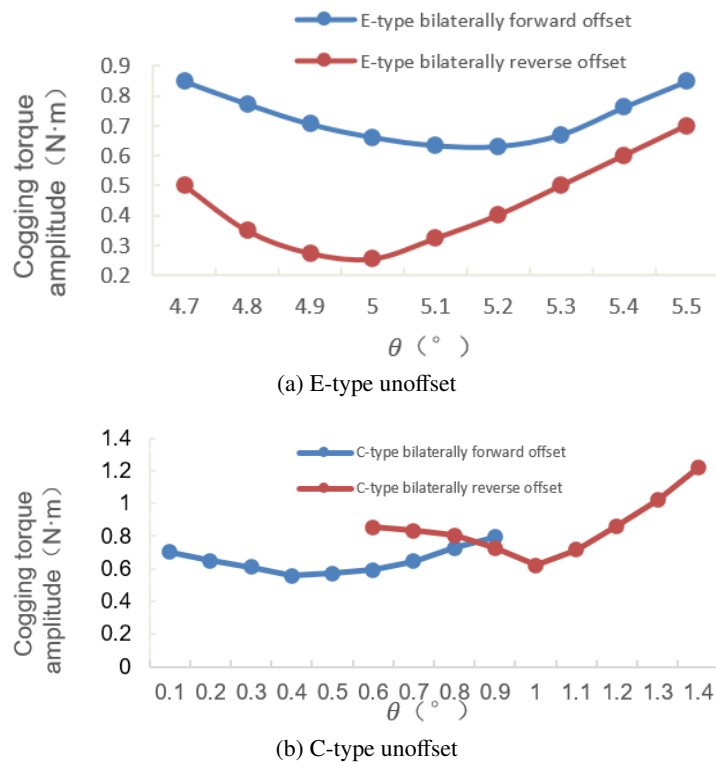

(a) E-type unoffset

(b) C-type unoffset

Fig. 8. Cogging torque at different offset angles

Figure 8 shows that the weakening effect is most pronounced when the values of θ for the E-type bilaterally reverse offset, E-type bilaterally forward offset, C-type bilaterally reversed offset, and C-type bilaterally forward offset models are 5°, 5.2°, 1°, and 0.4°, respectively. These values were used in subsequent simulations.

3.2. Cogging torque simulation

Figure 9 shows a comparison of the simulation results for the cogging torque of E-type bilaterally reverse offset and E-type bilaterally forward offset in one cycle. Figure 8 shows that the cogging torque of the E-type bilaterally reverse offset motor is reduced by 80.52% compared to the unoffset motor, and the cogging torque of the E-type bilaterally forward offset motor is reduced by 51.91% compared to the unoffset motor. Therefore, both E-type bilaterally reverse offset and E-type bilaterally forward offset can significantly reduce the cogging torque of the motor.
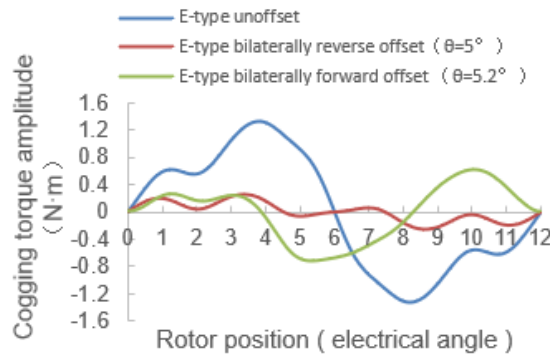

Fig. 9. Comparison of E-module schemes

Figure 10 shows a comparison of the simulation results for the cogging torque of the C-type bilaterally reverse offset and C-type bilaterally forward offset in one cycle. The results show that the cogging torque of the C-type bilaterally reverse offset motor is reduced by 14.86% compared
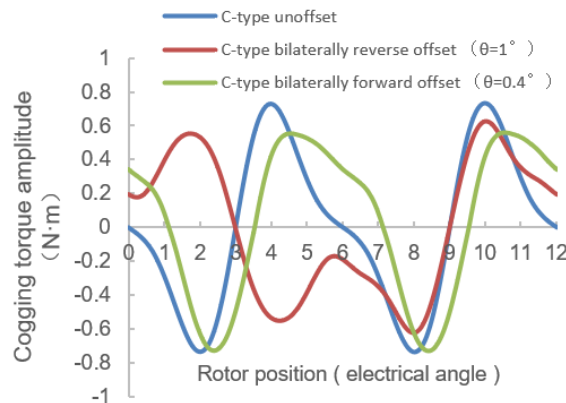

Fig. 10. Comparison of C-type module schemes

to the unoffset motor, while the cogging torque of the C-type bilaterally forward offset motor is reduced by 23%. The cogging torque of the motor is reduced by both the C type bilateral reverse offset and the C type bilateral forward offset. Because the fact that the distance between the C type modules is twice as large as the number of E type modules, resulting in a relatively small reduction in cogging torque.

4. Electromagnetic performance and vibration simulation

The analysis focuses on the electromagnetic performance and vibration noise of the motor. It is noted that the stator tooth groove and gap offset have a more pronounced effect on the magnetic circuit of the modular motor.

4.1. No-load air-gap flux density

The air gap magnetism of a permanent magnet motor can be separated into radial and tangential components. It is worth noting that the tangential air gap magnetism value is relatively small in comparison [25]. Therefore, only the radial unloaded air gap magnetism will be analysed. The operating wave of the motor's air-gap magnetic density is related to the pole-slot fit. In this case, the 10-pole, 12-slot motor operates with a 5th wave. Figure 11 displays the simulation results of radial no-load air gap magnetism for each model, while Fig. 12 shows the harmonic content of air gap magnetism for each model. Table 2 presents a comparison of the parameters for each model.

Table 2. Comparison of air gap flux density parameters

Parameter	Irregularity of waveform	Effective value (T)	Maximum value (T)
E-type unoffset	25.50%	0.5096	0.8010
E-type bilaterally reverse offset	30.30%	0.5029	0.7101
E-type bilaterally forward offset	30.88%	0.5045	0.9103
C-type unoffset	31.05%	0.4935	0.8584
C-type bilaterally reverse offset	31.03%	0.4936	0.9970
C-type bilaterally forward offset	31.06%	0.4922	0.8539

When combined with Fig. 11 and Table 2, it is evident that the E-type module results in an increase in the harmonic component of the air-gap magneto-density after the gap offset. This increase is due to the large gap offset, and it causes the waveform distortion rate to increase by approximately 5%. However, the RMS value remains largely unaffected. The air gap magnetism amplitude decreases by 12.47% for the E-type bilaterally reverse offset module, and increases by 13.64% for the E-type bilaterally forward offset module.

The C-type module has a smaller air gap offset, resulting in a smaller harmonic component of the air gap magnetism, and the waveform distortion rate has almost no effect on the RMS value. The magnitude of the air gap magnetism increases by 16.14% for the C-type bilaterally reverse offset module, while it remains almost unchanged for the C-type bilaterally forward offset module.

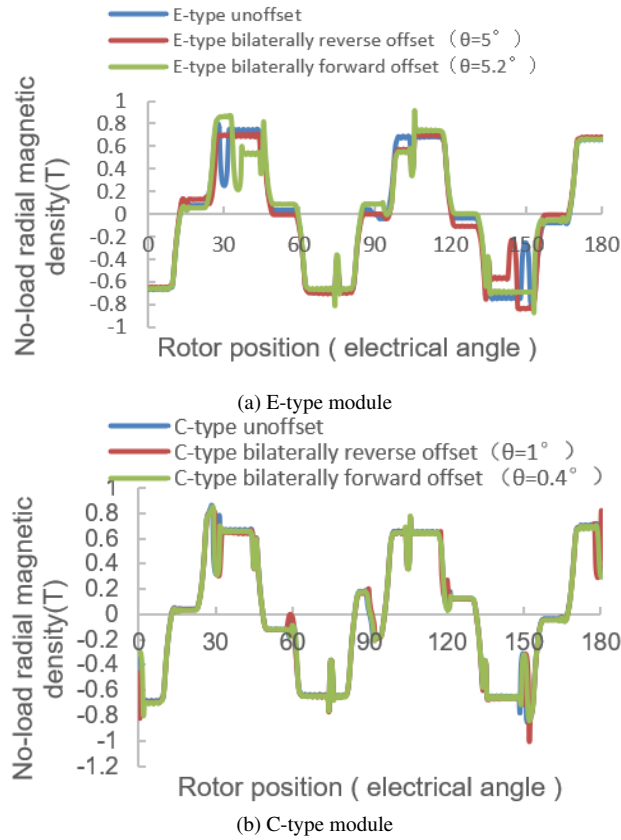(a) E-type module

(b) C-type module

Fig. 11. Radial no-load air gap flux density

Figure 12 shows that for a motor with fractional slot winding and 10-pole and 12-slot coordination, the operating wave is the 5th wave, with main harmonic components being the higher odd harmonics such as 7th, 15th, and 25th.
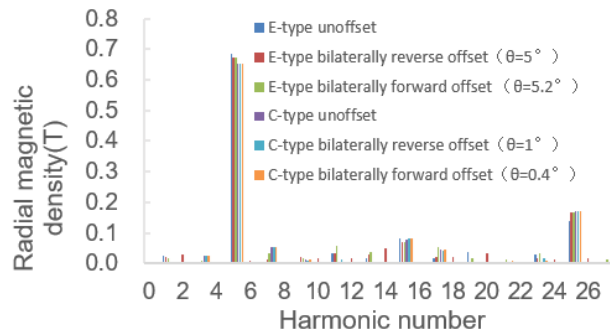

Fig. 12. Harmonic content of no-load air gap flux density

4.2. No-load reverse electromotive force

Figures 13 and 14 display the no-load reverse potential waveforms and harmonic content of the reverse potential in phase A for each model during one cycle at rated speed. Table 3 compares the reverse potential parameters of each model. It is evident that the motor's harmonic components are primarily concentrated in the 3rd, 5th, 7th, 9th, and 11th harmonics. After applying the gap offset treatment, the larger offset angle of the E-type module results in a significant impact on its 3rd harmonic. This causes a decrease in the waveform distortion rate of the E-type bilaterally reversed offset model by 3.5%, a decrease in RMS value by 1.5%, and a decrease in amplitude by 0.5%. Conversely, the waveform distortion rate of the E-type bilaterally forward offset model increases by 3.62%, RMS value increases by 1.96%, and amplitude increases by 6.59%.
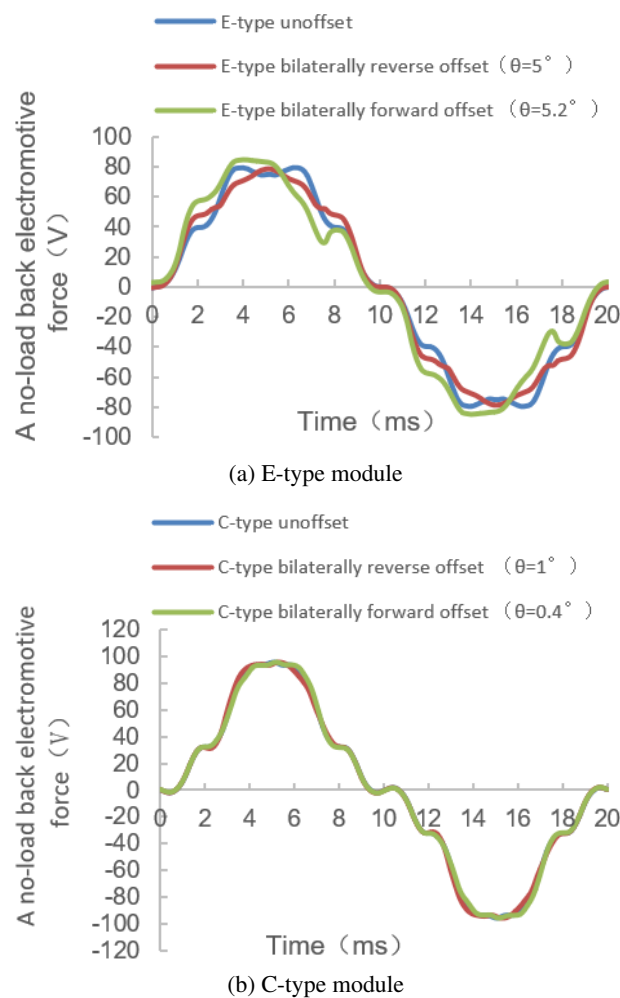

(a) E-type module

(b) C-type module

Fig. 13. No-load back electromotive force

Due to the small offset angle of the C-type module, the offset operation had almost no effect on it.

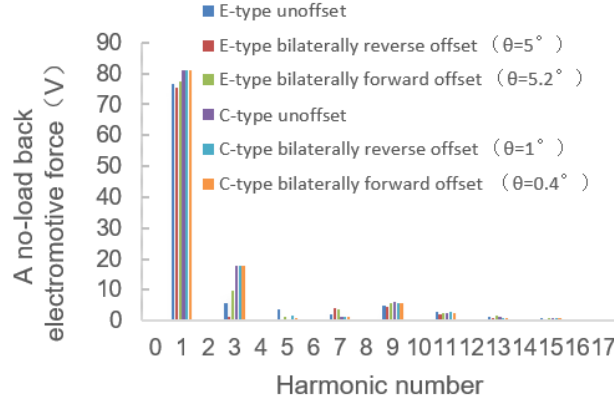Fig. 14. Harmonic content of back electromotive force

Table 3. Comparison of back electromotive force parameters

Parameter	Irregularity of waveform	Effective value (V)	Maximum value (V)
E-type unoffset	12.17%	54.45	79.26
E-type bilaterally reverse offset	8.67%	53.63	78.83
E-type bilaterally forward offset	15.79%	55.52	84.49
C-type unoffset	23.50%	59.01	95.28
C-type bilaterally reverse offset	23.35%	58.97	95.28
C-type bilaterally forward offset	23.58%	59.02	95.42

4.3. Output torque

Figure 15 displays the output torque waveforms for the designed motor models when connected to the same rated current. Table 4 compares the output torque parameters for each model.

The torque pulsation coefficient for the article is defined as

$$T_{\mathrm{ripple}} = \Delta T_{\mathrm{pp}}/T_{\mathrm{avp}}, \tag{16}$$

where T_{ripple} is the torque pulsation coefficient, ΔT_{pp} is the peak-to-peak value of output torque, T_{avp} is the average output torque.

It is evident that the torque pulsation coefficient for the E-type module is significantly reduced after offset, with both values decreasing by 41.67%. The maximum value is reduced by 6.86% and the average torque remains almost unchanged. However, for the C-type bilaterally reverse offset module, the torque pulsation coefficient is increased by 42%. After offset, the maximum value
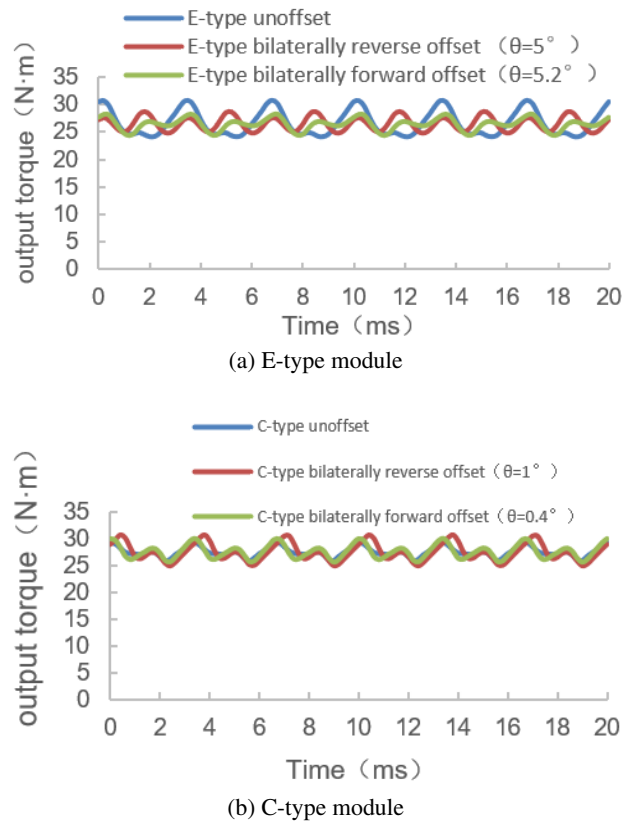
(a) E-type module

(b) C-type module

Fig. 15. Output torque

Table 4. Comparison of output torque parameters of each model

Parameter	Torque ripple	Average (N·m)	Max (N·m)
E-type unoffset	0.12	26.63	30.75
E-type bilaterally reverse offset	0.07	26.52	28.64
E-type bilaterally forward offset	0.07	26.40	28.20
C-type unoffset	0.07	27.51	29.40
C-type bilaterally reverse offset	0.10	27.36	30.57
C-type bilaterally forward offset	0.07	27.59	30.01

increases by 3.97% and the average value remains almost unchanged. Similarly, for the C-type bilaterally forward offset module, the maximum value increases by 2.07% and the torque pulsation coefficient remains almost unchanged from the average value.

4.4. Noise analyses

The motor's noise sources can be broadly classified as aerodynamic noise, mechanical vibration noise, and electromagnetic vibration noise [26]. The gap offset mainly affects the electromagnetic vibration noise; therefore, only the electromagnetic noise is analyzed.

Figure 16 shows the multi-rotational speed sound pressure level waterfall obtained by using simulation software Ansys Workbench to simulate the E and C modules respectively at 1m from the rotating axis under the rated current, with the rotational speed ranging from 100 rpm to 3000 rpm.

(a) E-type unoffset

(b) C-type unoffset

(c) E-type bilaterally reverse offset

(d) C-type bilaterally reverse offset

(e) E-type bilaterally forward offset

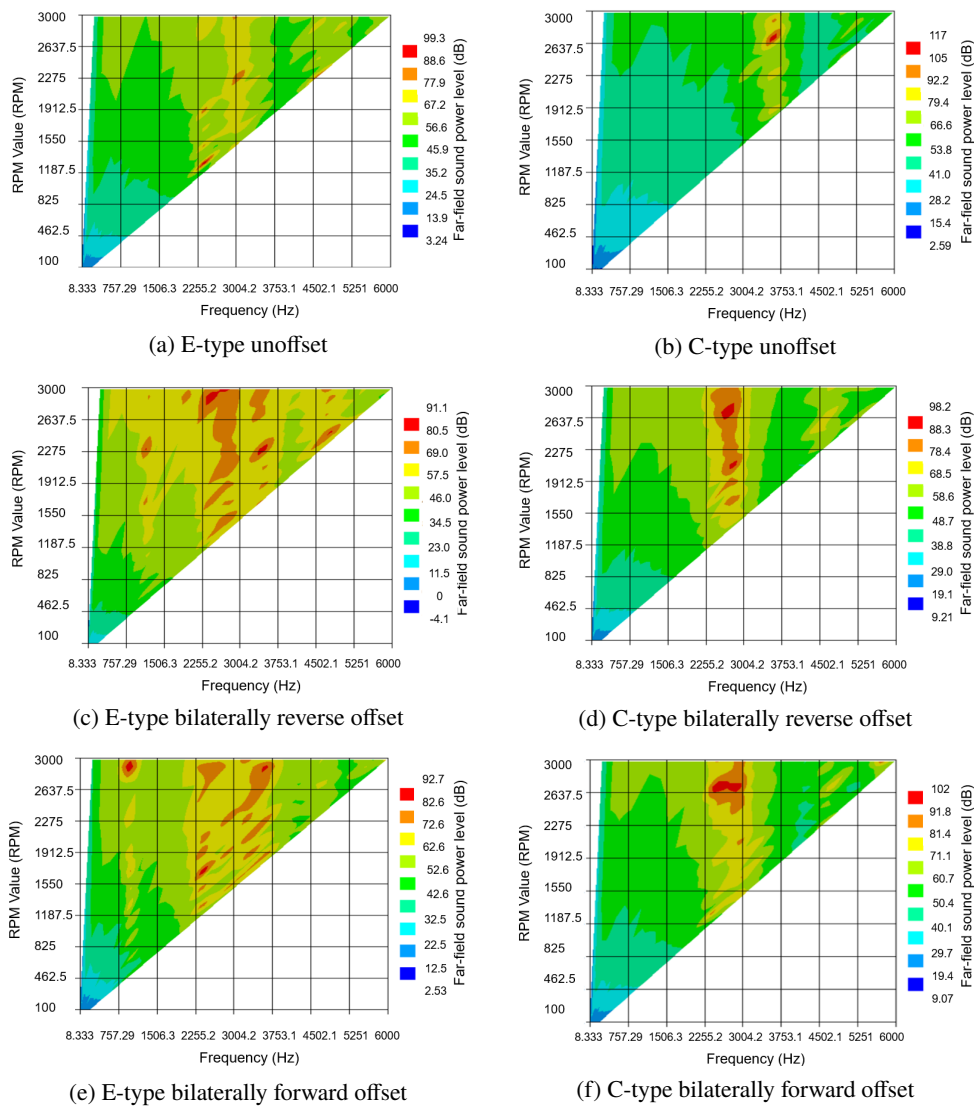(f) C-type bilaterally forward offset

Fig. 16. Multi-speed sound pressure level waterfall diagram

Figure 16 illustrates that the noise amplitude of the E-type module is primarily concentrated within the sound frequency range of 2255–3753 Hz. The noise amplitude is 99.3 dB when it is not offset. This occurs at a speed of 1300 rpm and a sound frequency of 2383.3 Hz. The noise amplitude of the E-type bilaterally reverse offset module is 91.1 dB, which is 8.25% lower than that of the unshifted module. This occurs at a speed of 2300 rpm and a sound frequency of 3450 Hz. The E-type bilaterally forward offset module produces a noise amplitude of 92.71 dB, which is 6.63% lower than the unshifted module. This occurs at a speed of 2900 rpm and a sound frequency of 966 Hz.

The noise amplitude of the C-type module is primarily concentrated within the sound frequency range of 2255–3753 Hz. The noise amplitude is 117.8 dB when it is not offset. This occurs at a speed of 2700 rpm and a sound frequency of 3600 Hz. The noise amplitude of the C-type bilaterally reverse offset module is 98.26 dB, which is 16.58% lower than that of the unshifted module. This occurs at a speed of 2700 rpm and a sound frequency of 2700 Hz. The C-type bilaterally forward offset module produces a noise amplitude of 102.15 dB, which is 13.28% lower than the unshifted module. This occurs at a speed of 2700 rpm and a sound frequency of 2475 Hz.

Taken together, both methods reduce the electromagnetic vibration noise of the motor during offset operation.

5. Conclusion

This paper proposes two schemes for modular motor gap offset to reduce cogging torque. The effectiveness of these schemes is verified through finite element simulation. Additionally, the paper analyses important parameters that affect the motor. The results indicate that:

1. For the E-type module, both schemes can significantly reduce cogging torque, while having minimal impact on other parameters. Additionally, they can also reduce electromagnetic vibration noise of the motor.

2. For the C-type module, the doubling of the number of gaps results in a relatively small weakening effect on the two schemes for cogging torque, but there is still some impact. Additionally, due to the smaller gap offset angle requirements, the impact on other parameters is also smaller. Furthermore, the electromagnetic vibration and motor noise weakening is better than that of the E-type module.

   The bilaterally reverse offset module scheme can have a greater cogging torque weakening effect compared to other parameters, but it is not significantly different from the bilaterally forward offset module scheme. However, the bilaterally reverse offset module scheme requires the use of two types of stator modules, which increases the processing and assembly requirements. Under the premise of considering economic factors, it is preferred to use the bilaterally forward offset module scheme. Otherwise, the bilaterally reverse offset module scheme is preferred.

References

[1] Tian Yi, *Design and analysis of split-stator permanent magnet motor*, North China: North China Electric Power University (in Chinese) (2020), DOI: 10.27139/d.cnki.ghbdu.2020.000156.

[2] Kung Wang, Baochang Xie, Xu Cai, *Modular stator permanent magnet wind turbine and its control*, Motor and Control Applications (in Chinese), vol. 45, no. 11, pp. 104–109 (2018), DOI: 10.3969/j.issn.1673-6540.2018.11.018.

[3] Li T., Zhang Y., Liang Y., *Multiphysics Analysis of an Axial-Flux In-Wheel Motor with an Amorphous Alloy Stator*, IEEE Access, vol. 8, pp. 27414–27425 (2020), DOI: 10.1109/ACCESS.2020.2972017.

[4] Baker N.J., Smith D.J.B., Kulan M.C., Turvey S., *Design and Performance of a Segmented Stator Permanent Magnet Alternator for Aerospace*, in IEEE Transactions on Energy Conversion, vol. 33, no. 1, pp. 40–48 (2018), DOI: 10.1109/TEC.2017.2739201.

[5] Akita H., Nakahara Y., Miyake N., Oikawa T., *New core structure and manufacturing method for high efficiency of permanent magnet motors*, 38th IAS Annual Meeting on Conference Record of the Industry Applications Conference 2003, Salt Lake City, UT, USA, vol. 1, pp. 367–372 (2003), DOI: 10.1109/IAS.2003.1257527.

[6] Chen Z., Spooner E., *A modular, permanent-magnet generator for variable speed wind* turbines, 1995 Seventh International Conference on Electrical Machines and Drives (conf. publ. no. 412), Durham, UK, pp. 453–457 (1995), DOI: 10.1049/cp:19950913.

[7] Zhu Z.Q., Azar Z., Ombach G., *Influence of Additional Air Gaps Between Stator Segments on Cogging Torque of Permanent-Magnet Machines Having Modular Stators*, IEEE Transactions on Magnetics, vol. 48, no. 6, pp. 2049–2055 (2012), DOI: 10.1109/TMAG.2011.2179667.

[8] El-Refaie M., *Fractional-slot concentrated windings synchronous permanent magnet machines: Opportunities and challenges*, IEEE Transactions on Industrial Electronics, vol. 57, no. 1, pp. 107–121 (2010), DOI: 10.1109/TIE.2009.2030211.

[9] El-Refaie M., Shah M.R., *Comparison of induction machine performance with distributed and fractional-slot concentrated windings*, Industry Applications Society Annual Meeting, pp. 1–8 (2008), DOI: 10.1109/08IAS.2008.30.

[10] Dajaku G., Gerling D., *Low costs and high-efficiency electric machines*, 2012 2nd International Electric Drives Production Conference (EDPC), Nuremberg, Germany, pp. 1–7 (2012), DOI: 10.1109/EDPC.2012.6425093.

[11] Wang Aimeng, Zhang Li, Li Heming, *Design and Application of High Performance Permanent Magnet Synchronous Motor Servo Control System*, Journal of North China Electric Power University (in Chinese), vol. 38, no. 4, pp. 13–17 (2011), DOI: 10.13462/j.cnki.mmtamt.2019.03.037.

[12] Jiang C., Qiao M., Zhu P., Zheng Q., *Design and Verification of High Speed Permanent Magnet Synchronous Motor for Electric Car*, 2018 2nd IEEE Advanced Information Management, Communicates, Electronic and Automation Control Conference (IMCEC), Xi'an, China, pp. 2371–2375 (2018), DOI: 10.1109/IMCEC.2018.8469398.

[13] Gerlando A.D., Perini R., Ubaldini M., *High pole number, PM synchronous machine with concentrated coil armature windings*, Springer Netherlands, pp. 1–6 (2006), DOI: 10.1007/978-1-4020-4535-6_26.

[14] Bianchi N., Bolognani S., *Design techniques for reducing the cogging torque in surface-mounted PM motors*, IEEE Transactions on Industry and Applications, vol. 38, no. 5, pp. 1259–1265 (2002), DOI: 10.1109/TIA.2002.802989.

[15] Bianchi N., Bolognani S., Grezzani G., *Object-oriented algorithms for automatic finite element analysis of PM motors*, Second International Conference on Power Electronics, Machines and Drives (PEMD 2004), Edinburgh, UK, vol. 2, pp. 817–822 (2004), DOI: 10.1049/cp:20040394.

[16] Li Shanshan, Wang Aimeng, *Influence of stator gap width on electromagnetic performance of permanent magnet motor*, Electrical Measurement and Instrumentation (in Chinese), vol. 61, no. 1, pp. 1–9 (2023), DOI: 10.19753/j.issn1001-1390.2024.01.010.

[17] Lu Wenkai, Zhang Wei, Zhao Xianfeng, *Influence of assembly clearance on cogging torque of modular permanent magnet motor*, Combined Machine Tool and Automatic Machining Technology (in Chinese), vol. 541, no. 3, pp. 143–145+148 (2019), DOI: 10.13462/j.cnki.mmtamt.2019.03.037.

[18] Wang Dongliang, Chen Wei, *Research on single-tooth block concentrated winding permanent magnet synchronous traction machine*, Explosion-proof Motor (in Chinese), vol. 55, no. 1, pp. 7–9+20 (2020.

[19] Dajaku G., Gerling D., *A novel 12-teeth/10-poles PM machine with flux barriers in stator yoke*, 2012 XXth International Conference on Electrical Machines, Marseille, France, pp. 36–40 (2012), DOI: 10.1109/ICElMach.2012.6349835.

[20] Huang Shoudao, Liu Ting, Ouyang Honglin, *Method of reducing cogging torque of permanent magnet motor based on slot offset*, Journal of Electrical Technology (in Chinese), vol. 28, no. 3, pp. 99–106 (2013), DOI: 10.19595/j.cnki.1000-6753.tces.2013.03.014.

[21] Wang Aimeng, Li Shanshan, Li Dashuang, *Influence of different stator modular structures on the performance of fractional-slot permanent magnet motor*, Motor and Control Applications (in Chinese), vol. 49, no. 3, pp. 54–59+66 (2022), DOI: 10.12177/emca.2021.170.

[22] Liu Ting, Ouyang Honglin, Huang Shoudao, *Reducing cogging torque of permanent magnet wind turbine based on repetitive unit*, Journal of Electrical Technology (in Chinese), vol. 26, no. 12, pp. 43–48 (2021), DOI: 10.19595/j.cnki.1000-6753.tces.2011.12.007.

[23] Wang Zheng, *Block and hinge brushless DC motors*, Micromotors (in Chinese), vol. 38, no. 5, pp. 16–18+21 (2010), DOI: 10.3969/j.issn.1004-7018.2010.05.005.

[24] Baranski M., *Comparative analysis of the power parameters of a line start permanent magnet synchronous motor using professional FEM packages and in-house software*, Archives of Electrical Engineering, vol. 72, no. 3, pp. 585–596 (2023), DOI: 10.24425/aee.2023.146038.

[25] Ibrahim I., Lowther D.A., *A Study of the Relationship between Acoustic Noise and Torque Pulsation in Permanent Magnet Synchronous Motors*, 2022 IEEE 20th Biennial Conference on Electromagnetic Field Computation (CEFC), Denver, CO, USA, pp. 1–2 (2022), DOI: 10.1109/CEFC55061.2022.9940912.

[26] Liu Kai, Zhang Bingyi, Feng Guihong, *Research on vibration and noise characteristics of double-sided rotor permanent magnet synchronous motor based on armature tooth offset method*, Journal of Electrical Technology (in Chinese), vol. 36, no. 1, pp. 95–106 (2021), DOI: 10.19595/j.cnki.1000-6753.tces.l90187.

Correction information:

The surname of the last co-author in the presented paper was incorrect in its original pdf version, published on September 24, 2024. This has been corrected in the current pdf version of the manuscript published on November 05, 2024.